Comparison of Optimization Strategy and Similarity Metric in Atlas-to-subject Registration Using Statistical Deformation Model

Y. Otake[a,c], R. J. Murphy[b], R. B. Grupp[a], Y. Sato[c], R. H. Taylor[a], M. Armand[b]
[a]Department of Computer Science, Johns Hopkins University, Baltimore MD, USA
[b]Johns Hopkins University Applied Physics Laboratory, Laurel MD, USA
[c]Graduate School of Information Science, Nara Institute of Science and Technology, Nara, Japan

ABSTRACT

A robust atlas-to-subject registration using a statistical deformation model (SDM) is presented. The SDM uses statistics of voxel-wise displacement learned from pre-computed deformation vectors of a training dataset. This allows an atlas instance to be directly translated into an intensity volume and compared with a patient's intensity volume. Rigid and non-rigid transformation parameters were simultaneously optimized via the Covariance Matrix Adaptation – Evolutionary Strategy (CMA-ES), with image similarity used as the objective function. The algorithm was tested on CT volumes of the pelvis from 55 female subjects. A performance comparison of the CMA-ES and Nelder-Mead downhill simplex optimization algorithms with the mutual information and normalized cross correlation similarity metrics was conducted. Simulation studies using synthetic subjects were performed, as well as leave-one-out cross validation studies. Both studies suggested that mutual information and CMA-ES achieved the best performance. The leave-one-out test demonstrated 4.13 mm error with respect to the true displacement field, and 26,102 function evaluations in 180 seconds, on average.

Keywords: Statistical deformation model: atlas-to-subject registration: evolutionary optimization.

1. INTRODUCTION

There is a wealth of literature investigating statistical atlases for a variety of applications [1]. Typical examples of atlas application are learning anatomical shape variation to infer abnormalities and longitudinal changes in patients, and patient-specific surgical planning or diagnosis. The adaptation of an atlas to a patient image, also known as atlas-to-subject registration [2], is performed by searching, via numerical optimization, for deformation parameters that maximize the similarity between a deformed atlas and a subject image. Statistical models have commonly been constructed with point distribution models (PDMs). Learning statistical variation and constructing a low dimensional subspace typically follows a linear dimensionality reduction such as principal component analysis (PCA). In order to reduce the search complexity, rigid and non-rigid transformation parameters are typically optimized separately in successive stages via a local search strategy with a linearized objective function; however, such optimization may suffer from local optima due to a highly multimodal objective space, thus requiring an initialization close to the global solution.

We propose a robust atlas-to-subject registration method using an evolutionary optimization strategy, reducing sensitivity to initialization. The method employs an atlas learned via PCA of voxel-wise displacement vectors, also known as a statistical deformation model (SDM)[3]. The atlas instance is directly translated into an intensity image rather than via a PDM approach, enabling direct comparison through an image similarity metric. The highly parallelizable nature of this algorithm allows an efficient implementation on environments such as GPUs, which enable a significant number of function evaluations, and facilitate simultaneous estimation of both rigid and non-rigid transformation parameters.

Furthermore, we challenge our algorithm to perform registration of the atlas to partial (incomplete) volumes of the organ of interest. This is especially useful in situations where obtaining the full image of the organ may be unnecessary for diagnosis and prohibitive due to radiation concerns, but useful for image-guided intervention procedures. One motivating example is developmental hip dysplasia where obtaining a full CT pelvis scan is not necessary for diagnosis, especially since the patients undergoing the corrective surgery (e.g., periacetabular osteotomy (PAO)) are usually young females. Performing computer assisted PAO surgery, however, will benefit from availability of the CT image of the whole pelvis [4].

Medical Imaging 2015: Image-Guided Procedures, Robotic Interventions, and Modeling,
edited by Ziv R. Yaniv, Robert J. Webster III, Proc. of SPIE Vol. 9415, 94150Q
 · doi: 10.1117/12.2081754

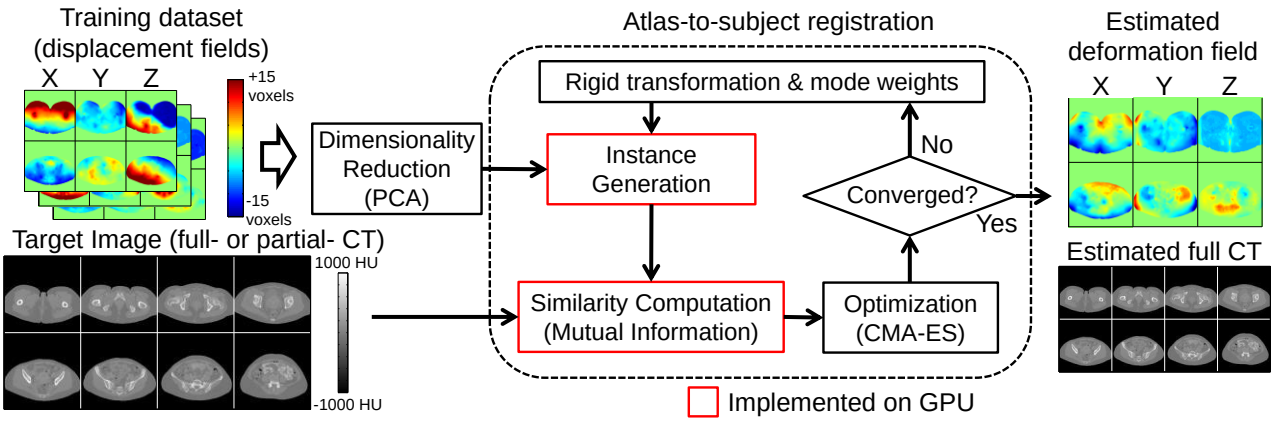

Fig. 1. Flowchart of the proposed non-rigid registration algorithm

2. METHODS

2.1 Overview of the proposed method

The proposed registration method is summarized in Fig. 1. Using pre-computed displacement vectors for each training subject, an SDM is constructed. The optimization in atlas-to-subject registration searches rigid transform and non-rigid (mode weight parameter) spaces, yielding an image that has maximum similarity with the target image. The following sections detail each component of the framework.

2.2. Preprocessing and displacement field computation

The training data in this study consisted of 55 CT volumes (256 × 256 × 148 voxels, 1.53 mm^3) of female hips (from the proximal femur to the superior aspect of the pelvis). Isomap analysis [5] performed on the training dataset prior to selecting a template subject minimized potential bias. The subject closest to the subspace origin was chosen as the template [6]. Given a subject image, $s(\boldsymbol{x})$, and a template image, $t(\boldsymbol{x})$, a non-rigid registration algorithm finds a mapping, $d: \mathbb{R}^3 \rightarrow \mathbb{R}^3$, such that $s(\boldsymbol{x} + d(\boldsymbol{x})) \cong t(\boldsymbol{x})$. In this study, the mapping was found using SyN, a symmetric diffeomorphic fluid based registration implemented in the Advanced Normalization Tools (ANTs) software package [7]. ANTs was highly ranked in a comparison among publicly available registration algorithms [8].

2.3. Principal Component Analysis on voxel-wise displacement vectors

For each subject, $i = 1 \cdots N$ (N: number of subjects), and for each voxel in the displacement field (n total voxels), the X, Y, and Z components of each displacement vector, d, are stacked together to form a long vector, $D_i \in \mathbb{R}^{3n}$. PCA using eigenvalue decomposition was performed on the vectors, $\{D_i, i = 1 \cdots N\}$, and principal components are computed as in eq. 1.

$$D(\boldsymbol{\lambda}) = \overline{D} + \sum_{j=1}^{M} \lambda_j \boldsymbol{p}_j \quad (1)$$

$D(\boldsymbol{\lambda})$ is a vector representing the displacement field parameterized by the weight vector $\boldsymbol{\lambda}$, M is the number of principal modes, $\overline{D}$ is the mean displacement field, $\boldsymbol{p}_j$ is the jth principal mode, and λ_j is the jth mode weight. For improved performance, the matrix-matrix multiplication function `cublasSgemm` (in CUBLAS library, nVidia) computed multiple evaluations of eq. 1 in parallel.

2.4. Atlas-to-subject registration

A moving image, $I_{moving}(x)$, is computed by applying the displacement field and a 6 degree-of-freedom rigid transformation to the template image,

$$I_{moving}(x) = t\big(x + d(Rx + T)\big) \quad (2)$$

where $d(x)$ is the displacement field computed in eq. 1 (i.e., 3 elements of $D(\boldsymbol{\lambda})$ corresponding to each voxel), R and T are 3 degrees of freedom rotational and translational components of the rigid transformation. A bicubic interpolation kernel implemented on the GPU using the CUDA library efficiently performed the voxel-wise operation in eq. 2.

Atlas-to-subject registration seeks a weight vector $\hat{\boldsymbol{\lambda}}$ and a rigid transform, $\hat{T}, \hat{R}$, yielding a moving image best matching the target image, I_{target}, as in eq. 3.

$$\{\hat{T}, \hat{R}, \hat{\boldsymbol{\lambda}}\} = \underset{T,R,\boldsymbol{\lambda}\in C}{\operatorname{argmax}} SM\left(I_{target}, I_{moving}(D(\boldsymbol{\lambda}), R, T)\right) \quad (3)$$

C is a user-specified parameter representing the search space, and SM represents the similarity metric. Note that the target image, I_{target}, may be a partially acquired image, which is one potential application scenario mentioned above. Furthermore, applying a projective transform to the moving image (i.e., creating a digitally reconstructed radiograph of I_{moving}), I_{target} may be a 2D projection image, leading to a 2D-3D application such as in [9].

We tested two similarity metrics, mutual information (MI) and normalized cross correlation (NCC), both implemented on the GPU. MI uses the `atomicAdd` operation to compute the joint histogram and reduction operation to compute the summation. NCC utilizes the CUBLAS library to perform computation on multiple images in parallel by treating a series of images as one matrix

The optimization design compared Covariance Matrix Adaptation Evolutionary Strategy (CMA-ES) [10], used to achieve robustness against local optima, with one conventional algorithm popular in derivative-free optimization—Nelder-Mead downhill simplex (NM-Simplex)[11]— which is intrinsically sequential. CMA-ES simultaneously evaluates multiple sample points (population size) in each generation. Sample points are randomly generated based on a normal distribution determined by a covariance matrix that is determined (adapted) in each generation. The parallel function evaluation significantly improved computational performance in our GPU implementation. The design parameters for the optimization is shown in Table 1.

Table 1. Design parameters for the optimization

Parameters for CMA-ES	
Population size (λ)	100
Upper/lower bound of search space	Translation: ±50 mm, Rotation: ±20 deg Mode weights: $\pm 3\sigma$
Initial search distribution (σ)	0.4 × search range (upper bound – lower bound)
Parameters for NM-Simplex	
Initial simplex size	Translation: 50 mm, Rotation: 20 deg Mode weights: 3σ
Parameters common for both algorithms	
Downsampled image size	128 × 128 × 74 voxels (3.0^3 mm^3)
Convergence criteria	Tolerance of function value: 0.1 Maximum function evaluation: 30,000
Initialization	Zero for all parameters (mean shape)

2.5. Error metrics

Two types of error metrics were used: 1) "displacement error," representing the average magnitude difference between the true and estimated displacement vectors, i.e., $e_d = \frac{1}{n}\sum_{j=1}^{n}\left\|\boldsymbol{d}_j - \widehat{\boldsymbol{d}_j}\right\|$, where $\widehat{\boldsymbol{d}_j}$ is the true displacement vector of the jth voxel and 2) "shape mode error", representing average absolute difference between the true and estimated mode weights, i.e., $e_\lambda = \frac{1}{M}\sum_{j=1}^{M}\left|\lambda_j - \widehat{\lambda_j}\right|$, where $\widehat{\lambda_j}$ is the true mode weight of the jth mode. Note that λ was normalized by the standard deviation of each mode.

2.6. Experiments

Simulation study. A displacement field was synthesized using eq. 1 with a randomly generated rigid transformation and 50 random mode weights. Using these parameters, the synthetic target image was created from the template image with eq. 2. The atlas-to-subject registration was computed on the synthetic target image, and the estimated displacement field was compared with the true displacement field. The optimization was performed with a variable number of modes (5 to 50) to investigate the dependency of performance with respect to the number of variables. The experimental protocol is summarized in Table 2.

Table 2. Simulation study protocol

Number of modes used to synthesize	50
Range of random variables (translation, rotation, mode weights)	(±50 mm, ±20 deg, ±3σ)
Number of modes used in optimization	5, 10, 15, …, 50
Similarity metric	MI, NCC
Optimization algorithm	CMA-ES, NM-Simplex

Leave-one-out cross validation. PCA was performed on the training dataset excluding one subject. A deformation field of the left-out subject was estimated with the proposed algorithm and compared with the true deformation field. The true mode weights were computed by projecting the subject onto each principal vector ($\boldsymbol{p}_i$). In order to evaluate the potential application regarding the extrapolation of missing structures, a partial CT scan was simulated by replacing all voxels in a contiguous section of slices with -1000 HU (i.e., air). Three different partial scan scenarios were tested, with 30%, 50%, and 70% of the original slices removed (Fig. 2).

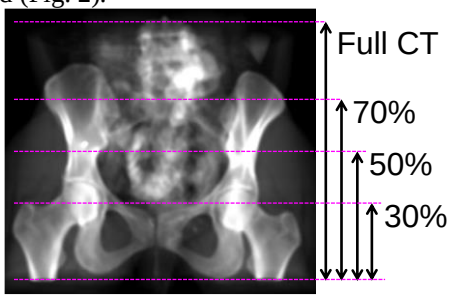

Fig. 2. Partial CT volume definition for leave-one-out cross validation experiments.

3. RESULTS

3.1. Simulation study

Results of the simulation study using synthetic subjects are summarized in Fig. 3. Ten random trials were conducted for each experimental setup. The box plot shows the 25th to 75th percentiles, the median (red line), the minimum and maximum (whisker plot), and the outliers (red cross). CMA-ES demonstrated higher accuracy than NM-Simplex for both displacement and shape mode error. MI performed slightly better than NCC for both optimization methods, suggesting the information theoretic metric better captured similarity even when both images are the same modality. Since the target images were generated using 50 modes, estimations using less than 50 modes yielded residual error. For CMA-ES & MI with 50 modes used, the median displacement error, e_d, was 0.86 mm, the median absolute shape mode error was 0.16, the average computation time was 191.42 sec, and averaged 28,082 function evaluations (146.7 function evaluations per second). NM-Simplex converged with fewer function evaluations; however, it was less robust against local optima and computationally inefficient—with 50 modes, NM-Simplex averaged convergence in 3,268 function evaluations over 97.68 sec.

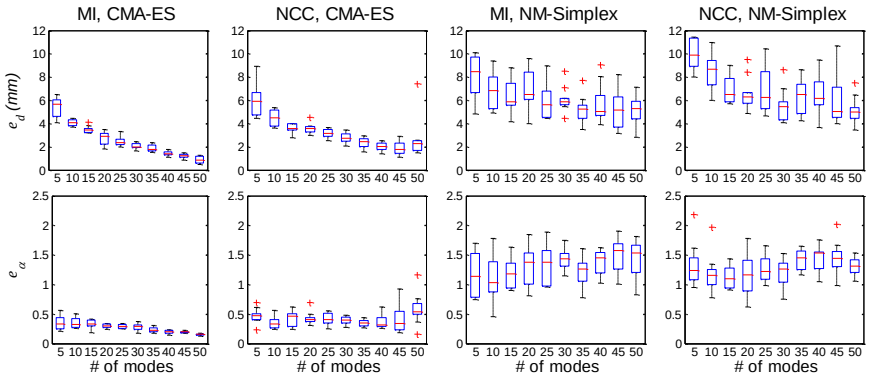

Fig. 3. Results of the simulation study using synthetic subjects: the upper row shows the displacement error as a function of number of PCA modes used, and the lower row shows the shape mode error. CMA-ES with MI clearly outperformed the other setups

3.2. Leave-one-out cross validation

Fig. 4 shows the results of the leave-one-out cross validation study. One box plot represents the result of 55 leave-one-out tests, where one subject was left out at a time. The optimization was performed with 50 modes. The median displacement error with CMA-ES & MI was 4.13 mm and the shape error was 0.37σ with 26,102 function evaluations in 180.0 sec on average. The error in displacement and mode weights increased as the amount of acquired slices decreased for the partial CT experiment with CMA-ES & MI as in Fig. 4c,d. The median displacement errors were 4.94 mm, 5.86 mm, and 7.81 mm for the 70%, 50%, and 30% partial CTs, respectively. Fig. 5 shows an example subject with displacement errors close to the median. Distribution of the displacement error was colormapped onto the estimated subject's surface mesh, showing a clear trend of increased error in regions where CT slices had been removed.

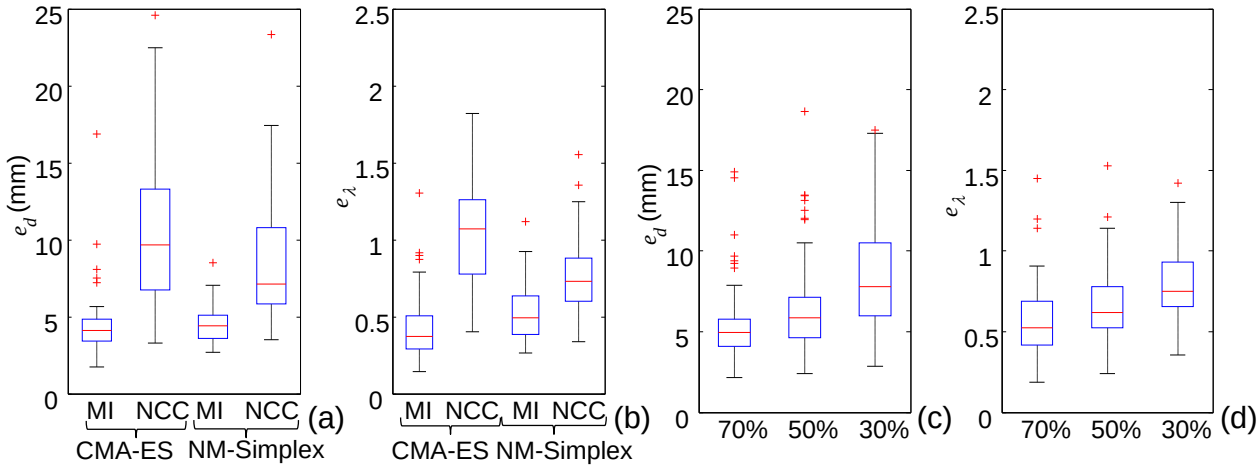

Fig. 4. Results of the leave-one-out cross validation study demonstrating (a) displacement and (b) shape parameter errors in each experimental setup, as well as (c) displacement and (d) shape parameter errors for the partial CT experiment using CMA-ES and MI.

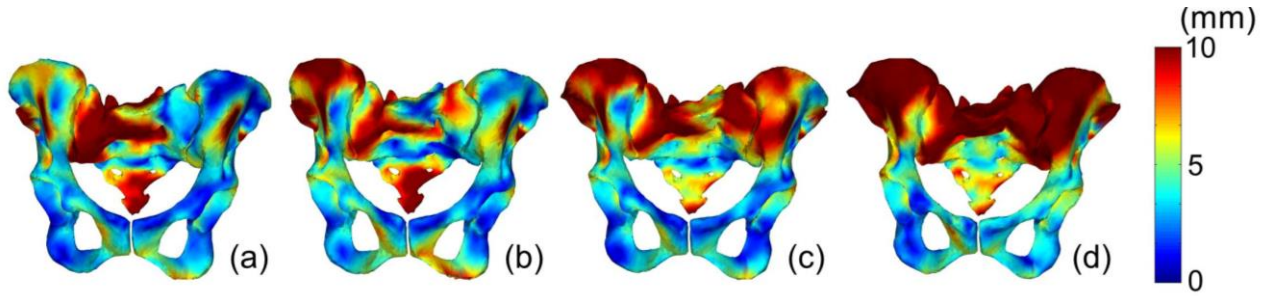

Fig. 5. Results of missing slice extrapolation using atlas-to-partial CT registration. Registration to (a) Full CT, (b) 70%, (c) 50%, (d) 30% partial CT (see Fig. 2). The surface mesh of the subject was estimated by applying displacement vectors to the template subject's mesh and the surface distance error with respect to the true subject is colormapped.

4. CONCLUSIONS

We have presented an atlas-to-subject registration method using SDM. The main contributions of this work are: 1) the application of an evolutionary optimization strategy in atlas-to-subject registration to simultaneously solve the rigid transformation and shape parameters, and 2) comparison with a conventional optimization strategy with two types of similarity metric. The evolutionary optimization allows for highly robust optimization, even with a large number of parameters (i.e., 6 rigid transformation parameters + 50 shape parameters). The proposed SDM-based registration framework enables flexible extensions, such as the extrapolation of missing image slices as shown above, or with intensity-based non-rigid 2D-3D registration. The large error around the iliac wing in the extrapolation experiment, especially when more than 50% of

data is missing (Fig. 5), suggests that merely using partial data may not be satisfactory for CT-based intraoperative registration during PAO surgery. The future work will investigate enhancing extrapolation by combining information from existing standing x-ray images into the partial CT data.

ACKNOWLEDGEMENT

This work is partially supported by NIH/NIBIB R01EB016703 grant.

REFERENCES

1. Heimann, T. and H.-P. Meinzer: Statistical shape models for 3D medical image segmentation: A review. Medical Image Analysis. 13(4): p. 543-563, (2009).
2. Ellingsen, L.M., et al.: Robust deformable image registration using prior shape information for atlas to patient registration. Comput Med Imaging Graph. 34(1): p. 79-90, (2010).
3. Rueckert, D., Frangi, A. F., & Schnabel, J. A. Automatic construction of 3-D statistical deformation models of the brain using nonrigid registration. IEEE Trans Med Imaging, 22(8), 1014-1025. (2003).
4. Chintalapani, G., et al.: Statistical Atlas Based Extrapolation of CT Data. Medical Imaging 2010: Visualization, Image-Guided Procedures, and Modeling. 7625, (2010).
5. Tenenbaum, J.B., V.d. Silva, and J.C. Langford: A Global Geometric Framework for Nonlinear Dimensionality Reduction. Science. 290(5500): p. 2319-2323, (2000).
6. Hamm, J., C. Davatzikos, and R. Verma, Efficient Large Deformation Registration via Geodesics on a Learned Manifold of Images, in Medical Image Computing and Computer-Assisted Intervention – MICCAI 2009, p. 680-687 (2009).
7. Avants, B.B., et al.: A reproducible evaluation of ANTs similarity metric performance in brain image registration. Neuroimage. 54(3): p. 2033-2044, (2011).
8. Klein, A., et al.: Evaluation of volume-based and surface-based brain image registration methods. Neuroimage. 51(1): p. 214-220, (2010).
9. Sadowsky, O., G. Chintalapani, and R.H. Taylor: Deformable 2D-3D registration of the pelvis with a limited field of view, using shape statistics. Med Image Comput Comput Assist Interv. 10(Pt 2): p. 519-26, (2007).
10. Hansen, N., The CMA Evolution Strategy: A Comparing Review, in Towards a New Evolutionary Computation, p. 75-102 (2006).
11. Nelder, J.A. and R. Mead: A Simplex Method for Function Minimization. The Computer Journal. 7(4): p. 308-313, (1965).